Effect of nanosilica-based activators on the performance of an alkali-activated fly ash binder

Erich D. Rodríguez[1*], Susan A. Bernal[2†], John L. Provis[2†*], Jordi Paya[1], José M. Monzo[1], and María Victoria Borrachero[1*]

[1] Instituto de Ciencia y Tecnología del Hormigón, Universitat Politècnica de València, 46022 Valencia, Spain

[2] Department of Chemical and Biomolecular Engineering, University of Melbourne, Victoria 3010, Australia

[†]Current address: Department of Materials Science and Engineering. University of Sheffield, Sheffield, United Kingdom.

* To whom correspondence should be addressed. Email: errodnar@disca.upv.es, erichdavidrodriguez@gmail.com (EDR); j.provis@sheffield.ac.uk (JLP)

phone: +34-963 877 007 (75648), fax: +34-963 877 569

Abstract

This paper assesses the effect of the use of an alternative activator based on nanosilica/MOH (M= K^+ or Na^+) blended solutions on the performance of alkali-activated fly ash binders. Binders produced with commercial silicate activators display a greater degree of reaction, associated with increased contents of geopolymer gel; however, mortars produced with the alternative nanosilica-based activators exhibited lower water demand and reduced permeability, independent of the alkali cation used. Na-based activators promote higher compressive strength compared with K-based activators, along with a refined pore structure, although K-activated samples exhibit reduced water demand. Zeolite type products are the major crystalline phases formed within these binders. A wider range of zeolites is formed when using commercial silicate solutions compared with the alternative activators. These results suggest that there are variations in the availability of Si in the system, and consequently in the alkalinity, depending on the silicate source in the activator, which is important in determining the nanostructure of the geopolymer gel.

Keywords: Alkali-activated binders, soluble silicate solutions, nanosilica, X-ray diffraction, scanning electron microscopy

1. Introduction

Interest in the development of alternative building materials such as alkali-activated binders has been promoted by the growth of the building industry, the increased performance requirements placed upon materials, and the higher sustainability criteria applied in construction. Alkali-activated binders represent an attractive alternative for the partial or complete substitution of Portland cement in the production of mortars and concretes, offering comparable performance and cost [1] while reducing greenhouse gas emissions [2]. Specifically, the alkali-activation of low calcium fly ashes (FA) has been extensively assessed over the past decades because these binders exhibit mechanical performance comparable to that reported for Portland cement, and because FA is an industrial by-product available worldwide. FA is produced in high amounts, especially in countries such as India and China, where an increased demand for cement is expected in the coming years. Despite the promising properties of these binders, and their ongoing commercialization, there are technological challenges associated with the variability of the raw materials from different sources, and the low sustainability of the current alkali-activators used [3].

In the activation of aluminosilicate precursors such as FA, the nature of the activator solution plays a key role in determining structural and mechanical performance. The most relevant characteristics related to the alkali activator are: the type of alkaline salt (usually silicate or hydroxide) [4-6]; the method of addition of the alkaline component (as a solution or in solid-state) [7-9], and the dosage of the alkali component, usually expressed as molar ratios considering the overall composition of the raw material. Additionally, it has been reported [4, 10-11] that the alkali cation supplied by the alkaline solution influences the first stages of binder formation, and consequently the mechanical performance of the final products. The alkali-activators conventionally used are sodium or potassium hydroxides, and/or sodium or potassium silicates [12]. Activation with K-containing solutions often leads to increased compressive strength development when compared with Na-containing solutions, where the size and charge density of the alkali cation play an important role in controlling the rate and extent of condensation during the polycondensation or crystallization process [13]. However, these effects are also dependent on the chemical and physical nature of the solid precursor used [5].

69   The embodied energy associated with the preparation of an alkali-activated binder is often

70   estimated based on the contributions of the precursor and the alkaline activator. Some

71   studies have analyzed the real energy consumed in fly ash based geopolymer production

72   [14-15], identifying that the major contribution is associated with the type and

73   concentration of the alkaline activator, and is between 0.5 MJ/t and 3.4 MJ/t. This is

74   mainly related to the complex chemical processes required to manufacture these

75   substances. For instance, the production of sodium silicate involves the calcination of

76   sodium carbonate (Na_2CO_3) and quartz sand (SiO_2) at temperatures between 1400-1500ºC,

77   producing large amounts of CO_2 as a secondary product [16-18]. This substantially

78   increases the embodied energy of silicate-activated binders, reducing sustainability.

79   However, sodium silicate ($Na_2O \cdot rSiO_2$, sometimes referred to as 'waterglass') is the

80   activator which generally provides the highest compressive strength development at early

81   ages of curing, and exhibits some technological advantages compared with other activators

82   such as NaOH.

83

84   This then provides motivation for the examination of the current activators used in

85   geopolymerization processes in terms of their sustainability, and the assessment of

86   alternatives that can contribute to reducing the embodied energy of these binders. Some

87   studies assessing alternative activators based on modified silica fume (MSF) have been

88   conducted [19-21]. Likewise, agro-industrial wastes, as well as other silica sources, have

89   been studied as alternative alkali-activators in order to obtain a more environmentally

90   friendly alkali-activated binder with lower cost [22-27]. These results reveal that this

91   alternative activator promotes similar or even better mechanical performance when

92   compared with conventional activators.

93

94   Based on this background, the aim of this paper is to study alkali-activated low calcium fly

95   ash binders, activated by chemically modified nanosilica. The effect of the alkali cation

96   (Na^+ and K^+) on the structure of the binders is studied by X-ray diffraction (XRD),

97   thermogravimetry and electron scanning microscopy (SEM/EDS). Compressive strength

98   testing and mercury intrusion porosimetry (MIP) are conducted on mortar samples based

99   on the binders produced, in order to generate a better understanding of the effect of the

100   type of activator used, the gel structure formed, and the mechanical strength development

101   of the materials.

102

2. Experimental program

2.1. Materials

The binders studied here were synthesized using a fly ash (FA) from Teruel Power Station in Andorra, Spain, with a specific gravity of 2520 kg/m^3 and a chemical composition as shown in Table 1. The FA was mechanically treated in a high impact mill (Mill2 Gabbrielli) to increase its reactivity. The particle size range determined by laser granulometry was 0.2-80 μm, with a mean particle size of 15 μm, and a specific surface of 1130 m^2/kg.

Table 1. Chemical composition of the fly ash from X-ray fluorescence analysis. LOI is loss on ignition at 950 ˚C

The X-ray diffraction pattern of the FA (Figure 1) shows that the major crystalline phases present are quartz (SiO_2; Powder Diffraction File (PDF) card # 00-046-1045), mullite ($Al_6Si_2O_{13}$; PDF# 00-015-0776), and Fe-rich phases such as hematite (Fe_2O_3; PDF# 00-033-0664), iron silicate (Fe_7SiO_{10}; PDF# 00-022-1118), and some ferrite spinels (magnetite - Fe_3O_4; PDF#00-019-0629, with and without substituent elements such as Mg and Al on both Fe^{2+} and Fe^{3+} sites). The presence of these phases is coherent with the high content of iron in the fly ash and has been previously observed in other fly ashes [28-30]. It is important to note that the ferrite spinels in the FA play an important role in the potential hosting of heavy metals, as Fe^{3+} sites can be substituted by trivalent cations such as Cr^{3+} [31].

Figure 1. Cu-K$_\alpha$ diffractogram of the fly ash after mechanical treatment

As alkali-activators, four alkaline solutions derived from hydroxide solutions and soluble silica sources were used. A commercial sodium silicate (SS) from Merck and a potassium silicate (SK) from IQE were used as reference soluble silica sources (Table 2). Two additional soluble silicates based on blends of a nanosilica suspension from H.S. Starck (L300, specific surface 300 m^2/g; Table 2) were also assessed. Alkali-activators were prepared by the dissolution of analytical sodium hydroxide (99 wt%) or potassium

136 hydroxide (85 wt%) pellets along with the silica source to obtain a molar oxide ratio
137 SiO_2/M_2O equal to 1.16, where M corresponds to Na^+ or K^+.
138
139 **Table 2**. Chemical composition of reference silicate activators and nanosilica used to
140 prepare nanosilica/MOH activators; data provided by the suppliers
141

142 *2.2.   Sample synthesis and test procedure*

143

144 *2.2.1. Pastes*
145 Alkali-activator with a molar oxide ratio SiO_2/M_2O of 1.16 was incorporated at 12.0 wt%
146 Na_2O or 18.2 wt% K_2O by mass of fly ash, providing equivalent alkali concentrations on a
147 molar basis for the samples prepared with different alkalis. All specimens were produced
148 by mechanical mixing for 4 minutes, including different contents of water in order to
149 obtain similar workability (Table 3)**.** It is important to note that the water/binder values
150 consider the liquids and solids contributed by both the activator and the precursor (i.e.
151 binder = fly ash + anhydrous activator).

152

153 **Table 3**. Mix description of silicate-activated fly ash binders

154

155 For the structural study of hardened pastes, the specimens were cast in cylindrical molds
156 and cured at a relative humidity (RH) of 90% and a temperature of 65ºC, for 48 h.
157 Afterwards, samples were kept in a high humidity atmosphere (RH $\geq$ 90%) at room
158 temperature (~25ºC). The reaction process was stopped at specified times by crushing the
159 samples and submerging them in acetone for 15 min, filtering and drying. In order to
160 prevent the carbonation of the powders thus obtained, these were stored in sealed
161 containers, and then analyzed:

162

163 • X-ray diffraction (XRD) was carried out using a Bruker D8 Advance instrument with
164 Cu Kα radiation and a nickel filter. The tests were conducted with a step size of 0.020º,
165 for a 2θ range of 3º to 65º.
166 • A thermobalance TGA-850 (Mettler Toledo) was used to analyze crushed samples at a
167 heating rate of 10ºC/min up to 1000ºC, with an alumina crucible in an dry air
168 atmosphere.

169 • Scanning electron microscopy (SEM) was conducted using a JEOL JSM6300

170 microscope with a tungsten filament electron source, and 20kV accelerating voltage.

171 The samples were evaluated in high vacuum mode. Attached to this instrument a Link-

172 Isis (Oxford Instruments) X-ray spectrometer system (energy dispersive spectroscopy

173 (EDS)) was used to determine the chemical compositions of the phases identified.

174

175 *2.2.2. Mortars*

176 Mortars were produced using a siliceous sand with a fineness modulus of 4.1 and specific

177 weight of 2680 kg/m^3, in accordance with the standard procedure UNE-EN 196-12005.

178 All samples were formulated with a standard fly ash:sand ratio of 1:3, cast in prismatic

179 moulds of 40×40×160 mm, compacted and mechanically vibrated for three minutes.

180 Curing was conducted in similar conditions as previously described for pastes; however,

181 after the period of curing at high temperature, mortars were stored in sealed containers at

182 RH ~90% and room temperature until testing. Compressive strength was determined after

183 2, 28 and 60 days following the standard testing protocol UNE-EN-1015-11. Additionally,

184 mercury intrusion porosimetry (MIP) was conducted after 28 days using an AutoPore IV

185 9500 (Micromeritics) instrument, with applied intrusion pressures between 13.8 kPa and

186 227.4 MPa.

187

188 **3. Results and discussion**

189

190 *3.1. Water demand*

191

192 From visual inspection, it was possible to identify that mixes produced with reference K-

193 based activators (commercial potassium silicate solution) exhibited increased workability

194 when compared with pastes produced with the reference Na-based activator (commercial

195 sodium silicate solution), which allowed a significant reduction of the total water included

196 in these binders while achieving a similar slump. Similar behavior has been reported in the

197 literature [5] for pastes prepared with K-based activators, which exhibit increased slump

198 compared to those prepared with Na-based activators. Additionally, the lower silica

199 content of the K-containing solutions will also have an effect in the fresh mixes, because

200 an increased content of silica in the alkali activator (higher Ms) causes reduced

201 workability of the fresh mixture, related to the higher viscosity identified in both Na and K

202 silicate solutions at increased silica concentrations [12].

203

204   The water demand of the binders prepared with the nanosilica-based activator is lower
205   than that of the pastes based on the reference silicate activators. Pastes including the
206   nanosilica-solution presented better workability than those prepared with commercial
207   silicate activator, independent of the alkali cation included in the solution, at an equivalent
208   M_2O/SiO_2 molar ratio. This is a consequence of the structural differences between the
209   nanosilica activator and the commercial silicate solutions. The low water demand of the
210   L300-K paste is particularly notable, where a water content less than half of that of the S-
211   Na sample is sufficient to provide good workability.

212

213   It is expected that in the commercial silicate solutions there will be a wide range of
214   dissolved silicate species, and among these, increased oligomer sizes affect the kinetics of
215   the exchange of silicate units during geopolymerization [32], contributing to an increment
216   in the viscosity of the solution, and consequently to the reduced workability of the
217   activated pastes. Conversely, in the nanosilica-derived activator, the rate of release of
218   soluble silicates is affected by the degree of dissolution of the particles in the hydroxide
219   solutions during the preparation of the activator. Considering that the time of preparation
220   of the activator is not longer than 5 hours before use (sufficient time for the solution to
221   cool to room temperature after the exothermic dissolution), not all of the nanosilica will be
222   completely dissolved in the hydroxide solution, and the oligomers formed in these silicates
223   might be lower in size compared to those in commercial silicates. This would then
224   decrease the viscosity of the nanosilica-derived activators, and consequently contribute to
225   the higher workability of the pastes produced with this activator, with reduced water
226   demand.

227

228   Improved workability associated with lower water demand in these binders is desirable
229   from a durability point of view, because a reduced degree of permeability of aggressive
230   agents through the hardened binders might be able to be achieved using these alternative
231   activators to enable the use of lower water/binder ratios. Detailed analysis of the pore
232   structure of these systems is presented later in this paper.

233

234

235

236

7

3.2. *Compressive strength*

All of the binders assessed show compressive strengths between 84 and 88 MPa after 2 days of curing at 65°C (Figure 2). These mortar compressive strength values enable the classification of these materials as high performance binders, considering that conventional Portland cement concretes with compressive strengths up to 60 MPa are classified as high performance, and to achieve these strengths generally requires the addition of chemical and/or mineral admixtures [33].

Figure 2. Compressive strength of alkali-activated fly ash mortars, as a function of the nature of the activator. Error bars indicate one standard deviation either side of the mean

As a consequence of the wide range of factors affecting the mechanical strengths of fly ash geopolymer binders, and the physical and chemical differences between fly ash and activator sources used by different research teams, it is difficult to make direct comparisons between the strengths reported by different authors. However, considering the relationship between the molar composition of the precursor and the mechanical strength proposed by Duxson and Provis [34], this ash will be expected to give good strength based on its chemical composition, which is coherent with the results reported here.

Mortars produced with Na-based activators present higher compressive strength than those with K-based activators. In both cases, slightly higher compressive strengths are obtained when using commercial silicates, especially at early ages. This effect is more notable in samples activated with the L300-K solution, which present compressive strengths up to 10MPa lower than the reference specimens (S-K). However, specimens prepared with the modified nanosilica activators present a clear linear trend in the strength development, so that at longer periods of curing (60 days) the compressive strengths of these mortars are comparable to those reported for the reference samples (S-Na and S-K).

These results are coherent with the mechanisms of activation which are known to take place when different alkali cations are incorporated in the binder. Xu *et al.* [35] observed that activation with NaOH promotes a higher degree of dissolution of aluminosilicate solids when compared with KOH. This is attributed to the higher capacity of NaOH to

271 favor the release of silicate and aluminate monomers [36-37], while K promotes
272 condensation reactions to a greater extent, leading to the presence of more polysilicate
273 species [13].

274

275 In alkali activation of metakaolin, the rate of reaction in alkaline K-enriched environments
276 is sufficient to promote a high extent of dissolution while favoring condensation of
277 reaction products at early ages [37]. This is one of the main reasons why, in metakaolin-
278 based geopolymers, increased compressive strengths are obtained using K silicate
279 activators compared with systems where Na silicate is the alkali source. Considering that
280 the rate of dissolution of fly ash in an alkaline environment is lower than that of
281 metakaolin [34], it might be expected that there would be a retardation of reaction kinetics
282 when using K-based activators. This is consistent with the lower compressive strength
283 development exhibited by S-K and L300-K samples. The slightly lower mechanical
284 strength values at early ages of curing reported for mortars prepared with the modified
285 nanosilica can be attributed to the lower dissolved silica content of the nanosilica/MOH
286 solutions compared with commercial silicate solutions, where the presence of remnant,
287 partially dissolved silica particles slows down the availability of SiO_2 in the system.

288

289 *3.3. Pore size distribution*

290

291 The MIP technique has some limitations related to measuring pore parameters in
292 cementitious materials due to the presence of different sizes and shapes of pores, where
293 deviations from cylindrical pore shapes will increase the measured volume of the very
294 small pores [38]. However, it is still a valuable technique providing information about the
295 threshold diameters and intrudable pore space, giving a better understanding of the effects
296 of the different activators on the connectivity and capacity of the pore structure in the
297 geopolymers assessed.

298

299 In general, K-geopolymers present lower total porosity than Na-geopolymer mortars, as
300 seen by the lower cumulative volume intruded (Figure 3). Also, the lowest porosity is
301 exhibited by samples prepared with the chemically modified nanosilica activator. Mortars
302 produced with the K-nanosilica activator (L300-K) reported a total porosity of 6.32%,
303 followed by those specimens produced with the Na-nanosilica activator (L300-Na) with a
304 total porosity of 9.75%. These results are consistent with the reduced water demand of the

9

305 chemically modified nanosilica-activated geopolymers, highlighting the benefit of using
306 this alternative activator.

307

308 **Figure 3.** Cumulative volume of mercury intruded as a function of pore diameter for S-
309 Na, L300-Na and L300-K mortars after 28 days of curing

310

311 The pore size distributions of the mortars assessed are presented in Figure 4, as calculated
312 from the applied pressure via the Washburn equation [39], assuming a contact angle of
313 130.0 degrees. In general, only slight differences are identified between the samples in
314 terms of the volumes of pores with diameters higher than ~10µm in samples prepared with
315 different alkali cations, despite the reduced water demand exhibited by K-activated
316 geopolymers compared with the Na-activated geopolymer mortars.

317

318 **Figure 4.** Pore size distributions obtained from mercury intrusion data for silicate-
319 activated fly ash mortars with 28 days of curing

320

321 A remarkable effect of the alkali cation on the pore size distribution is identified in the
322 region of diameters smaller than 1 µm, where an increased pore volume is reported for
323 L300-Na mortars compared with L300-K mortars. In this region two types of porosity can
324 be identified: macropores (50-200 nm) and mesopores (3.6-50nm). Mesopores are present
325 into the aluminosilicate gel network due to short-range ordering which is characteristic of
326 an amorphous material. Macropores are formed during the early stages of
327 geopolymerization, and may transform to mesopores with the progress of the
328 polycondensation of hydrated gels in the binders, as a consequence of the filling of the
329 larger pores with the new reaction products, particularly given the relatively high Ca
330 content of the fly ash used here. On the other hand, pores larger than 200nm in the
331 geopolymer pastes are likely to be associated with the interfacial spaces between partially-
332 reacted or unreacted fly ash particles and the geopolymer gel [38, 40]. It is important to
333 note that complete dissolution and reaction of precursors have never been observed in fly
334 ash geopolymer binders, in particular when the solid precursor contains unreactive
335 crystalline phases as is the case for the precursor used in the present study (Figure 1).

336

337 These results indicate that, although L300-Na mortars have higher water content and thus
338 report a higher total porosity than L300-K mortars, a higher extent of polycondensation of

10

339 the geopolymer gel is taking place in the presence of Na. This leads to the refinement of
340 the pore network, which contributes to the increased compressive strength. The presence
341 of pores of smaller diameter is important from a durability point of view, considering that
342 the diffusion of aggressive agents into the binders usually takes place through the larger
343 pores.

344

345 *3.4. X-ray diffraction*

346

347 In samples prepared with Na-based activators, the major crystalline phases previously
348 identified in the unreacted fly ash (Figure 1) are again observed; the crystalline
349 components of the fly ash are un-reactive. In pastes activated with commercial sodium
350 silicate, the main crystalline reaction products identified correspond to a calcium silicate
351 hydrate containing some sodium (N-C-S-H in cement chemistry terminology)
352 ($Na_2Ca_2Si_2O_7 \cdot H_2O$; PDF# 00-022-0891), analcime ($NaAlSi_2O_6 \cdot H_2O$); PDF# 00-002-
353 0417), gismondine ((Ca,Na_2)$Al_2Si_2O_8 \cdot 4H_2O$; PDF# 00-021-0840), Na-P1 zeolite
354 ($Na_2Al_2Si_2O_8 \cdot xH_2O$; PDF# 00-0025-0777) which is also a gismondine type structure,
355 along with the zeolites gonnardite ((Na,Ca)$_2(Si,Al)_5O_{10} \cdot 2H_2O$; PDF# 00-042-1381) and
356 mesolite ($Na_2Ca_2Al_5Si_9O_{30} \cdot 8H_2O$; PDF# 00-024-1064), which both present the natrolite
357 type structure. When activating with L300-Na, the Na-P1, analcime and N-C-S-H are not
358 identified; however, a new zeolite structure corresponding to faujasite
359 ($Na_2Al_2Si_{3.3}O_{10.6} \cdot 7H_2O$) (PDF# 00-012-0228) is detected. These zeolites have been also
360 formed in other fly ash geopolymer systems [41, 42] and through the hydrothermal
361 production of zeolites using a similar fly ash precursor [43, 44].

362

363 **Figure 5**. Cu-K$_\alpha$ diffractograms of the fly ash activated with Na-based activators. Peaks
364 present in both diffractograms are labeled in only one diffractogram for visual clarity.

365

366 The crystallization of zeolites from amorphous aluminosilicates is determined by the
367 dissolution rate of the precursor, which is controlled by at least two processes: (1) the
368 breakage of surface bonds due to the action of solvent and formation of soluble species
369 that leave the surface of the dissolving solid (directly proportional to the external surface
370 area), and (2) the reaction of the soluble species from the liquid phase on/with the surface
371 of the dissolving solid (depending only indirectly on the concentration of NaOH via the
372 change of the concentrations of reactive silicate and aluminate species in the liquid phase)

11

373 [34, 45]. Considering that all of the samples have been prepared with the same fly ash
374 precursor, it is likely that the structural differences are associated with variations in the
375 alkalinity provided by the different silicate activators.
376
377 In the hydrothermal preparation of pure analcime from pure silica and alumina sources at
378 intermediate alkalinity conditions, the Na-P1 zeolite has been identified in the early stages
379 of reaction, and it then exhibits a gradual dissolution while the crystallization of analcime
380 is taking place; however, increasing the alkalinity in the system favors the formation of
381 faujasite instead of Na-P1 or analcime [46]. Using the commercial silicates here, the
382 coexistence of analcime and Na-P1 zeolites is achieved, along with the formation of a
383 wide range of zeolites. This indicates that the activation conditions promoted by this
384 activator are favoring the nucleation and growth of stable crystalline zeolites. Conversely,
385 using the NaOH/nanosilica derived activator leads to a lower availability of SiO_2 species
386 in the systems, which is likely to maintain a higher alkalinity compared with commercial
387 silicate solutions at the early times of reaction, consequently promoting the formation of
388 faujasite.
389
390 Hajimohammadi et al. [47] studied geopolymer formation from systems with separate Si
391 and Al sources, and observed that analcime formation occurred in systems with low Si
392 availability, while faujasite development was promoted at intermediate or high rates of
393 high Si availability. This differs from the trends observed here, where reversed results are
394 obtained, indicating that the mechanisms of gel and zeolite nucleation and growth in
395 binders where Si and Al sources are separated differ from those where Si and Al are
396 provided in parallel by an aluminosilicate precursor (e.g. fly ash) along with an external
397 source of Si (activator). Considering that analcime is a relatively high-silica zeolite and its
398 formation is likely to occur in areas enriched in Si, it seems that the additional Si species
399 contributed by a highly dissolved activator can favor the formation of this phase when
400 using the commercial sodium silicate.
401
402 The use of commercial potassium silicate (S-K) (Figure 6) as activator also promotes the
403 formation of crystalline reaction products, such as lithosite ($K_3HAl_2Si_4O_{13}$; PDF# 00-037-
404 0457), K-cymrite ($KAlSi_3O_8 \cdot H_2O$; PDF# 00-016-0385) and aluminosilicate zeolites with a
405 chabazite-K type structure ($K_{10.9}Al_{11.1}O_{72}Si_{24.9} \cdot 25H_2O$; PDF# 00-037-0792). K-cymrite is
406 also identified in binders prepared with the L300-K activator, along with hydrodelhayelite

12

407 (KCa$_2$(Si$_7$Al)O$_{17}$(OH)$_2$.6H2O; PDF# 00-041-0611), and a chabazite-K zeolite

408 (KAlSiO$_4$.xH$_2$O; PDF# 00-053-1777). The formation of zeolite-like products including

409 calcium (in particular hydrodelhayelite; chabazite is also known to show Ca substitution,

410 although this was not explicitly observable here) is likely to be related to the weaker

411 zeolite structure forming tendencies of potassium here compared to sodium in Figure 5;

412 pure sodium zeolites form reasonably readily, while pure potassium zeolites are less

413 common, which leads to the formation of mixed-cation species as identified here.

414

415 **Figure 6**. Cu-K$_\alpha$ diffractograms of the fly ash activated with K-based activators. Peaks

416 present in both diffractograms are labeled in only one diffractogram for visual clarity.

417

418 *3.5.   Thermogravimetry*

419

420 The thermograms of the binders (Figure 7) after 28 days of curing exhibit an onset of

421 weight loss at temperatures lower than 300ºC, which is associated with the physically

422 bound and zeolitic water present in the reaction products (dominated by an aluminosilicate

423 type-gel) which can be easily removed from the sodium/potassium silicate gel surface at

424 these temperatures [48-50].   Loss of weight at temperatures higher than 300ºC is

425 consistent with dehydroxylation by condensation of the bound silanol groups, which is

426 completed at 500ºC [48].

427

428 **Figure 7.** Thermograms of silicate-activated fly-ash binders at 28 days of curing

429

430 Differences in the total weight loss are identified between samples with nanosilica-based

431 activators and commercial silicate activators. This is more marked when comparing

432 samples with different alkali cations, where geopolymers activated by Na salts presented a

433 total weight loss of ~13% while K-geopolymers presented ~11% weight loss. This is

434 consistent with the structural differences in the binders as identified by MIP and XRD as

435 discussed above. The total loss of weight in K-activated geopolymer paste is 18% lower

436 than in the Na-activated specimens, which is consistent with the difference in water

437 content between the samples. However, some of the additional weight loss reported for

438 Na-activated binders may also be attributed to a larger content of gel reaction products

439 having been formed at the time of curing at which these samples were assessed, compared

440 with K-activated samples. This is consistent with the higher compressive strength and

441 reduced permeability reported for Na-activated samples, independent of the silica source

442 in the activator.

443

444 Differential thermogravimetric curves (DTG; Figure 8) show a broad peak from room

445 temperature up to ~300ºC in all samples. The main peak identified in both S-Na and L300-

446 Na geopolymers presents a minimum at ~103ºC, attributed to the freely evaporable water

447 present in large pores in the geopolymer gel. The increased intensity of this peak in

448 samples activated with the commercial silicate solutions indicates a higher extent of

449 aluminosilicate gel formation, coherent with the high compressive strength identified in

450 mortars prepared with this binder. It is important to note that the first minimum related to

451 the loss of weight of evaporable water in these fly ash geopolymers (~103ºC) is at a higher

452 temperature than that which has been reported for metakaolin geopolymers (~58ºC) with

453 comparable formulations [50], indicating that the use of FA as a precursor for the

454 production of these binders favors the formation of denser geopolymer gels with tightly

455 absorbed water in small pores, or as condensed hydroxyl groups on the surface of the gel

456 [48, 51].

457

458 **Figure 8.** Differential thermograms of silicate-activated fly ash

459

460 In the samples S-Na and S-K a second peak is also observed at ~141ºC. In MK-based

461 geopolymers and activated MK/GBFS blends the presence of this second peak has been

462 associated with the dehydration of the zeolite-type product (hydroxysodalite in that case)

463 formed along with the geopolymer gel [50]. Oh et al. [52] reported that the geopolymer gel

464 formed through the alkali-activation of fly ash presents a disordered form of the ABC-6

465 family of zeolitic products, which contains different polytypes such as chabazite, and

466 ranging from amorphous structure to polycrystalline in the case of high alkalinity mixes.

467

468 Crystalline chabazite has previously been reported as a zeolitic product in sodium-fly ash

469 geopolymer systems [41]; however, crystalline chabazite structures are observed here

470 exclusively in samples with K-based activators (Figure 6). Weight loss of chabazite-type

471 zeolites has been reported at temperatures of 162ºC for chabazite-Na ("herschelite"), and

472 192°C for chabazite-K [53, 54], which probably indicates that the second peak identified

473 in DTG analysis of these binders (Figure 8) is likely to be related to geopolymer gel with a

474 chabazite-like nanostructure. A higher intensity of this peak is shown for pastes activated

475 with commercial silicates, which can be associated with the larger degree of reaction and
476 increased ordering of the gels formed.

477

478 A third peak at ~596ºC is only observed in commercial-silicate activated geopolymers (S-
479 Na and S-K), and is attributed to the complete dehydroxylation of zeolites present in the
480 binder. Conversely, a weaker signal at 509ºC, and a small and poorly defined peak at
481 490ºC are identified in L300-Na and L300-K binders respectively. The shifting of the
482 dehydroxylation peak towards lower temperatures is associated with lower alkali and Al
483 content, because of the greater strength of the bond between the water and the Na^+ or K^+
484 cations in this case [55, 56].

485

486 A low intensity peak at ~847ºC is identified in L300-K, corresponding to decomposition
487 of the carbonates, probably sodium or potassium carbonate (Figure 6). Similar peaks
488 (~780-800ºC) with reduced intensity are also exhibited by S-Na and S-K geopolymers.

489

490

491 *3.6. Scanning electron microscopy (SEM/EDS)*

492

493 Fly ash geopolymers activated with commercial sodium silicate (Figure 9) exhibit a
494 heterogeneous gel structure, with embedded particles of varying morphologies (Figure
495 9A): smooth spherical particles (Figure 9B), agglomerations of rectangular crystalline
496 particles mostly composed of Al and Si (Figure 9C) surrounded by an Si-rich gel,
497 spherical units formed from the agglomeration of tubular particles enriched in Fe (Figure
498 9D), and crystalline particles with a dendritic-type structure with a high content of Fe and
499 containing similar proportions of Al and Si (Figure 9E). Hollow cavities with spherical
500 shape are associated with the partial dissolution of fly ash particles during the
501 geopolymerization reaction, where the un-reacted remnant fly ash particles are not bound
502 to the geopolymer gel, and fall out from their positions in the cavities during sample
503 preparation for microscopic analysis.

504

505 In analysis of fly ashes from different sources [57], it has been identified that this material
506 presents a spherical particle shape, mostly consisting of amorphous aluminosilicate, along
507 with iron-rich spheres composed of iron oxide mixed with amorphous aluminosilicate with
508 variations in the contents of Al, Si and Fe. Specifically, the ferrospheres in fly ash present

15

509 a microstructure that can include smooth, polygonal, dendritic, granular and molten drop

510 characteristics [58], and can often be represented as a nanocomposite with ''core–shell"

511 structure, where the core is formed from spinel, hematite and quartz crystals (phases

512 observed by XRD in the fly ash used here), and the shell consists of glasses [59].

513

514 Considering the chemical compositions of the different phases forming the geopolymer

515 and the microstructural characteristics reported for unreacted fly ash, it is inferred that the

516 smooth spherical particles correspond to undissolved FA, while the agglomerated

517 rectangular particles are identifiable according to their composition as being mullite, and

518 those with dendritic-type structure are likely to be associated with the ferrite spinels

519 previously observed by XRD (Figure 5). This is coherent with the observations made by

520 Lloyd et al. [60] who identified remnant particles of un-reacted fly ash, along with

521 crystalline phases such as mullite, in fly ash-based geopolymers. This is attributed to the

522 differential solubilities of the phases composing the fly ash under the activation conditions

523 used, especially where those presenting high crystallinity are less soluble. In the fly ash

524 assessed, mullite has been identified by XRD, and is likely to be responsible for the

525 particles identified in Figure 9C.

526

527 **Figure 9.** Scanning electron micrographs and corresponding EDS spectra of the binder

528 activated with a commercial sodium silicate (S-Na)

529

530 Binders activated with the NaOH/nanosilica derived activator (Figure 10) present only

531 slight microstructural differences compared with commercial Na-silicate activated pastes.

532 In this case, it is also possible to identify a partially dissolved fly ash particle with a

533 needle-like phase over its surface (Figure 10B), which is rich in Al and Si. This phase is

534 likely to be associated with mullite crystals, including some Fe substituting for Al in the

535 mullite structure [61].

536

537 **Figure 10.** Scanning electron micrographs and corresponding EDS spectra for the binder

538 activated with NaOH/nanosilica-derived activator (L300-Na)

539

540 Dendritic type particles assigned to the ferrite spinels forming the unreacted FA are also

541 identified (Figure 10C), which is coherent with XRD (Figure 5). This is consistent with

542 the observations of Lloyd et al. [60] who observed that iron-rich phases in a fly ash

16

543   precursor are relatively unreactive. In this binder, a Ca- and Si-rich needle-like

544   morphology is visible inside one of the hollow cavities, presenting some traces of Na and

545   low contents of Al. Taking this into account, this morphology can be associated with some

546   sort of C-S-H phase. It is important to note that XRD results do not reveal the formation of

547   a long range-ordered C-S-H when using this activator; these phases are therefore

548   identifiable as showing at most short-range order.

549

550   The geopolymer gel embedding the different particles presents similar chemical

551   composition, independent of the silicate source, using Na-based activators. However, it

552   seems that there is a higher degree of interaction between this gel and the fly ash particles

553   in the binders prepared with the nanosilica-derived activator. This is coherent with the

554   reduced permeability exhibited by this binder (Figure 3), providing further evidence of the

555   effectiveness of using this alternative activator for producing geopolymers.

556

557   Binders prepared with a commercial K-silicate activator (Figure 11) also show mullite

558   crystals which were originally embedded within fly ash particles. As the reaction

559   progressed, the glass phase dissolved and exposed the mullite needles. Similarities in the

560   chemical composition of the geopolymer gel formed are again identified between the

561   samples which used the commercial K-silicate activator (Figure 11A) and the

562   KOH/nanosilicate derived activator (Figure 11B).

563

564   **Figure 11.** Scanning electron micrographs, and corresponding EDS spectra, of the binders

565   activated with (A) commercial potassium silicate solution (S-K) and (B) KOH/nanosilica

566   derived activator

567

568   **4.   Conclusions**

569

570   The production of high mechanical strength and low permeability geopolymers has been

571   achieved using alternative activators based on modified nanosilica. These binders show an

572   extent of reaction which is slightly lower than that of binders produced from the same fly

573   ash using commercial sodium silicate activators, but mechanical strengths are similar. The

574   water demand and porosity of the samples prepared with the nanosilica-based activators

575   are lower than for the case of the commercial silicate activators, which is attributed to the

576   slightly delayed release of silica from the solid nanosilica particles, which remain in

577 suspension in the solution during the early ages of reaction and then release silica later in
578 the reaction process. The crystalline zeolite phases formed in the samples differ slightly
579 between the nanosilica-derived and traditional activators, again consistent with the
580 differences in silica release rates from the two activators. Microstructural analysis shows
581 that the geopolymer gel is more tightly bound to the partially reacted fly ash particles in
582 the case of the nanosilica-derived activator, consistent with the reduced porosity of these
583 binders. The use of the nanosilica activator may also bring advantages in terms of the
584 environmental profile of the materials.
585

597 **References**
598

599 1. Duxson P., Fernández-Jiménez A., Provis J.L., Lukey G.C., Palomo A., van Deventer
600   J.S.J. Geopolymer technology: the current state of the art. J Mater Sci 2007, 42(9):
601   2917-2933.
602 2. Duxson P., Provis J.L., Lukey G.C., van Deventer J.S.J. The role of inorganic
603   polymer technology in the development of green concrete. Cem Concr Res 2007,
604   37(12): 1590-1597.
605 3. van Deventer J.S.J., Provis J.L., Duxson P., Brice D.G. Chemical research and climate
606   change as drivers in the commercial adoption of alkali activated materials. Waste
607   Biomass Valor 2010, 1(1):145-155.
608 4. van Jaarsveld J.G.S., van Deventer J.S.J. Effect of the alkali metal activator on the
609   properties of fly ash-based geopolymers. Ind Eng Chem Res, 1999, 38(10):3932-
610   3941,

611   5. Phair J.W., van Deventer J.S.J. Effect of silicate activator pH on the leaching and
612   material characteristics of waste-based inorganic polymers. Miner Eng 2001,
613   14(3):289–304.

614   6. Fernández-Jiménez A., Palomo A. Composition and microstructure of alkali activated
615   fly ash binder: Effect of the activator. Cem Concr Res 2005, 35:1984 – 1992

616   7. Yang K.-H., Song J.-K., Ashour A.F., Lee E.-T. Properties of cementless mortars
617   activated by sodium silicate. Constr Build Mater 2008, 22(9):1981-1989.

618   8. Yang K.-H., Song J.-K. Workability loss and compressive strength development of
619   cementless mortars activated by combination of sodium silicate and sodium
620   hydroxide. J Mater Civ Eng 2009, 21: 119-127

621   9. Hajimohammadi A., Provis J.L., van Deventer J.S.J. One-part geopolymer mixes from
622   geothermal silica and sodium aluminate. Ind Eng Chem Res. 2009, 47(23): 9396-
623   9405.

624   10. Duxson P., Mallicoat S.W., Lukey G.C., Kriven W.M., van Deventer J.S.J. The effect
625   of alkali and Si/Al ratio on the development of mechanical properties of metakaolin-
626   based geopolymers. Colloids Surf A 2007, 292(1): 8-20.

627   11. Fernández-Jiménez A., Palomo A., Criado M. Alkali activated fly ash binders. A
628   comparative study between sodium and potassium activators. Mater Constr. 2006,
629   56(281): 51-56.

630   12. Provis, J.L. Activating solution chemistry for geopolymers. In: Provis J.L., van
631   Deventer, J.S.J. (editors.) Geopolymers: Structures, Processing, Properties and
632   Industrial Applications, Woodhead Publishing, Abingdon UK, 2009, p50-71.

633   13. McCormick A.V., Bell A.T. The solution chemistry of zeolite precursors. Catal Rev
634   Sci Eng 1989, 31: 97-127.

635   14. Witherspoon R., Wang H., Aravinthan T., Omar T. Energy and emissions analysis of
636   fly ash based geopolymers. Proceedings of SSEE 2009 International Conference.
637   Melbourne, Australia, 2009.

638   15. Tempest B., Sanusi O., Gergely J., Ogunro V., Weggel D. Compressive strength and
639   embodied energy optimization of fly ash based geopolymer concrete. Proceedings of
640   the 2009 World of Coal Ash (WOCA) conference. Lexington, KY, USA, 2009.

641   16. McLellan B.C., Williams R.P., Lay J., van Riessen A., Corder G.D. Costs and carbon
642   emissions for geopolymer pastes in comparison to ordinary Portland cement. J
643   Cleaner Prod 2011, 19: 1080-1090.

19

644   17. Deabriges J. Process for the manufacture of sodium silicate. United States Patent
645   4,336,235, 1982.

646   18. Fawer M., Concannon M., Rieber W. Life cycle inventories for the production of
647   sodium silicates. Int J Life Cycle Assess 1999, 4(4): 207-212.

648   19. Živica V. High effective silica fume alkali activator. Bull Mater Sci 2004, 27(2): 179–
649   182.

650   20. Živica V. Effectiveness of new silica fume alkali activator. Cem Concr Compos 2006.
651   28(1): 21–25.

652   21. Rouseková I., Bajza A., Živica V. Silica fume-basic blast furnace slag systems
653   activated by an alkali silica fume activator. Cem Concr Res 1997, 27(12): 1825-182

654   22. Rodríguez E. Effect of Si/Al/Na/Ca ratio in geopolymeric materials based on
655   metakaolin. Master Thesis. Universidad del Valle. Cali, Colombia. 2008.

656   23. Rodríguez E. Effectiveness of alkali-activators based on different sources of silica for
657   the manufacture of fly ash geopolymer systems. Master Thesis. Universidad
658   Politécnica de Valencia, Spain. 2009.

659   24. Detphan S., Chindaprasirt P. Preparation of fly ash and rice husk ash geopolymer. Int
660   J Miner Metall Mater 2009, 16(6): 720-126.

661   25. Songpiriyakij S., Kubprasit T., Jaturapitakkul Ch., Chindaprasirt P. Compressive
662   strength and degree of reaction of biomass and fly ash-based geopolymer. Constr
663   Build Mater 2010, 24(3): 236-240.

664   26. Bernal S.A., Rodríguez E.D., Mejía de Gutiérrez R., Provis J.L., Delvasto S.
665   Activation of metakaolin/slag blends using alkaline solutions based on chemically
666   modified silica fume and rice husk ash. Waste Biomass Valor 2012, 3(1): 99-108.

667   27. Wongpa J., Kiattikomol K., Jaturapitakkul C., Chindaprasirt P. Compressive strength,
668   modulus of elasticity, and water permeability of inorganic polymer concrete. Mater
669   Des 2010, 31: 4748-4754.

670   28. Winburn R.S., Lerach S.L., McCarthy G.J., Grier D.G., Cathcart J.D. Quantification
671   of ferrite spinel and hematite in fly ash magnetically enriched fractions. Adv X-Ray
672   Anal 2000, 43: 350-355.

673   29. Vassileva S.V., Menendez R., Alvarez D., Diaz-Somoano M., Martinez-Tarazona
674   M.R. Phase-mineral and chemical composition of coal fly ashes as a basis for their
675   multicomponent utilization. 1. Characterization of feed coals and fly ashes. Fuel 2003,
676   82:1793–181

677   30. Williams R.P., van Riessen A. Determination of the reactive component of fly ashes
678   for geopolymer production using XRF and XRD. Fuel 2010, 89(12): 3683-3692.

679   31. Provis J.L., Rose V., Bernal S.A., van Deventer J.S.J. High-resolution nanoprobe X-
680   ray fluorescence characterization of heterogeneous calcium and heavy metal
681   distributions in alkali-activated fly ash. Langmuir 2009, 25(19): 11897–11904

682   32. Bahlmann E.K.F., Harris R.K., Rockliffe J.W., Smith E.G. Silicon-29 NMR self-
683   diffusion and chemical-exchange studies of concentrated sodium silicate solutions. J
684   Chem Soc, Faraday Trans. 1997, 93: 93-98.

685   33. Hewlett P.C. Lea's Chemistry of Cement and Concrete, 4th Ed. Elsevier, Oxford, UK,
686   1998

687   34. Duxson P., Provis J.L. Designing precursors for geopolymer cements. J Am Ceram
688   Soc 2008. 91(12): 3864-3869.

689   35. Xu, H., van Deventer, J.S.J., Lukey, G.C. Effect of alkali metals on the preferential
690   geopolymerization of stilbite/kaolinite mixtures. Ind Eng Chem Res 2001, 40(17):
691   3749-3756.

692   36. Duxson P., Lukey G.C., Separovic F., van Deventer J.S.J. Effect of alkali cations on
693   aluminium incorporation in geopolymeric gels. Ind Eng Chem Res 2005, 44(4): 832-
694   839.

695   37. Duxson P., Provis J.L., Lukey G.C., van Deventer J.S.J., Separovic F., Gan Z.H. ^{39}K
696   NMR of free potassium in geopolymers. Ind Eng Chem Res 2006. 45(26): 9208-9210.

697   38. Diamond S. Mercury porosimetry. An inappropriate method for the measurement of
698   pore size distribution in cement-based materials. Cem Concr Res 2000, 30: 1517-
699   1525.

700   39. Washburn E.W. Note on method of determining the distribution of pore sizes in
701   porous materials. Proc Nat Acad Sci U.S.A. 1921, 7(4): 115-116.

702   40. Kovalchuk G., Fernández-Jiménez A., Palomo A. Alkali-activated fly ash: Effect of
703   thermal curing conditions on mechanical and microstructural development – Part II.
704   Fuel 2007, 86: 315-322

705   41. Criado M., Fernández-Jiménez A., de la Torre A.G., Aranda M.A.G., Palomo A. An
706   XRD study of the effect of the SiO_2/Na_2O ratio on the alkali activation of fly ash.
707   Cem Concr Res 2007, 37: 671-679

708   42. Lloyd R.R. Accelerated ageing of geopolymers. In: Provis J.L, van Deventer, J.S.J.
709   (Eds.) *Geopolymers: Structures, Processing, Properties and Industrial Applications*,
710   Woodhead Publishing, Abingdon UK. 2009, p. 139-166.

711   43. Querol X., Alastuey A., Fernández-Turiel J.L., López-Soler A. Synthesis of zeolites
712   by alkaline activation of ferro-aluminous fly ash. Fuel 1995, 74(8): 1226-1231.

713   44. Querol X., Plana F., Alastuey A., López-Soler A. Synthesis of Na-zeolites from fly
714   ash. Fuel 1997, 76(8): 793-799.

715   45. Antonić T., Čižmek A., Subotić B. Dissolution of amorphous aluminosilicate zeolite
716   precursors in alkaline solutions: Part 2.- Mechanism of the dissolution. J Chem Soc
717   Faraday Trans 1994, 90(13): 1973-1977.

718   46. Kohoutková M., Kloužkova A., Maixner J., Mrázová M. Preparation and
719   characterization of analcime powders by X-ray and SEM analysis. Ceram–Silik 2007,
720   51(1): 9-14.

721   47. Hajimohammadi A., Provis J.L., van Deventer J.S.J. The effect of silica availability
722   on the mechanism of geopolymerisation. Cem Concr Res 2011, 41(3): 210-216.

723   48. Duxson P., Lukey G.C., van Deventer J.S.J. The thermal evolution of metakaolin
724   geopolymers: Part 1 – Physical evolution. J Non-Cryst Solids 2006, 352:5541-5555.

725   49. Duxson P., Lukey G.C., van Deventer J.S.J. The thermal evolution of metakaolin
726   geopolymers: Part 2 – Phase stability and structural development. J Non-Cryst Solids
727   2007, 353:2186-2200.

728   50. Bernal S.A., Rodríguez E.D., Mejía de Gutiérrez R., Gordillo M., Provis J.L.
729   Mechanical and thermal characterization of geopolymers based on silicate-activated
730   metakaolin/slag blends J Mater Sci. 2011, 46(16): 5477-5486.

731   51. Duxson P., Lukey G.C., van Deventer J.S.J. Physical evolution of Na-geopolymer
732   derived from metakaolin up to 1000˚C. J Mater Sci 2007, 42:3044-3054.

733   52. Oh J.E., Monteiro P.J.M., Jun S.S., Choi S., Clark S.M. The evolution of strength and
734   crystalline phases for alkali-activated ground blast furnace slag and fly ash-based
735   geopolymers. Cem Concr Res 2010, 40: 189-196.

736   53. Sticher H. Thermal analysis of synthetic (near-chabazite) zeolites with different Si/Al
737   ratios. Thermochim Acta 1974, 10: 305-311.

738   54. Stakebake J.L. Characterization of natural chabazite and 5A synthetic zeolites. Part 1.
739   Thermal outgassing properties. J Colloid Interf Sci 1984, 99(1): 41-49.

740   55. Mishin I.V., Piloyan G.A., Klyachko-Gurvich A.L., Rubinshtein A.M. Study of
741   decationized and dealuminized mordenites by the differential-thermal analysis method
742   and measurement of water vapour absorption. Russ Chem Bull 1973, 22(6): 1298-
743   1300.

744 56. Chandwadkar A.J., Kulkarni S.B. Thermal behaviour of modified faujasites. J
745   Thermal Anal 1980, 19: 313-320.

746 57. Kutchko B.G., Kim A.G. Fly ash characterization by SEM-EDS. Fuel 2006. 85:2537-
747   2544.

748 58. Xue Q.-F., Lu S.-G. Microstructure of ferrospheres in fly ashes: SEM, EDX and
749   ESEM analysis. J Zhejiang Univ Sci A 2008, 9(11): 1595-1600.

750 59. Zyryanov V.V., Petrov S.A., Matvienko A.A. Characterization of spinel and
751   magnetospheres of coal fly ashes collected in power plants in the former USSR. Fuel
752   2011, 90: 486-492.

753 60. Lloyd R.R., Provis J.L., van Deventer J.S.J. Microscopy and microanalysis of
754   inorganic polymer cements. 1: Remnant fly ash particles. J Mater Sci 2009, 44: 608-
755   619.

756 61. Gomes S., François M. Characterization of mullite in silicoaluminous fly ash by
757   XRD, TEM and ^{29}Si MAS NMR. Cem Concr Res 2000, 30:175-181.

758

759

760   **Table 1**. Chemical composition of the fly ash from X-ray fluorescence analysis. LOI is

761   loss on ignition at 950 ˚C

Component (weight % as oxide)	SiO_2	Al_2O_3	Fe_2O_3	CaO	MgO	SO_3	Na_2O	K_2O	LOI
Fly ash	39.00	28.01	15.43	10.27	1.50	2.00	0.71	1.38	1.69

762

763

764   **Table 2**. Chemical composition of reference silicate activators and nanosilica used to
765   prepare nanosilica/MOH activators; data provided by the suppliers

Component (weight % as oxide)	SiO_2	Na_2O	K_2O	H_2O	Solution modulus $(Ms)(SiO_2/M_2O)$
SS	28.7	8.7	-	62.4	3.30
SK	23.0	-	10.5	66.5	2.19
L300	35.7	-	-	64.3	-

766

767

768 **Table 3**. Mix description of silicate-activated fly ash binders

Properties	Mixture ID			
	S-Na	*S-K*	*L300-Na*	*L300-K*
alkali cation	Na^+	K^+	Na^+	K^+
silicate source	SS	SK	L300	L300
water/binder ratio	0.27	0.21	0.20	0.13

769

770
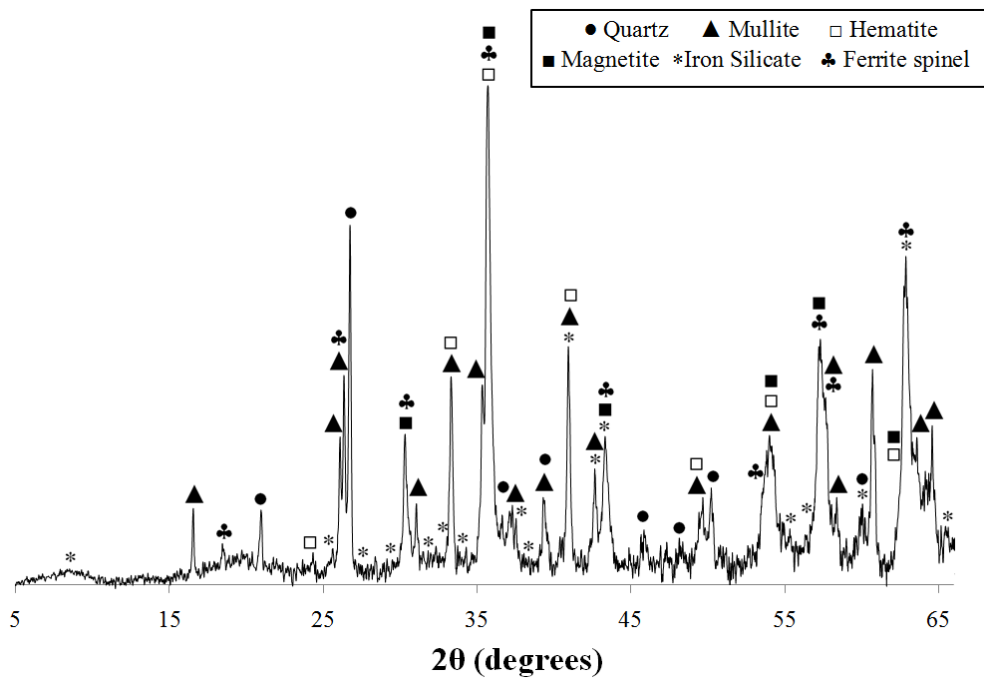
Figure 1. Cu-K$_\alpha$ diffractogram of the fly ash after mechanical treatment

774
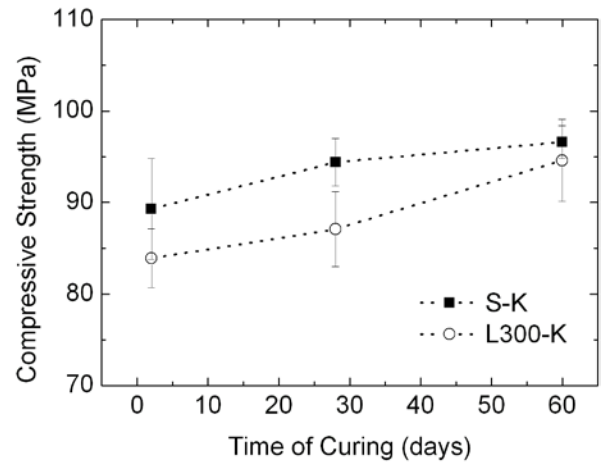
775

Figure 2. Compressive strength of alkali-activated fly ash mortars, as a function of the
nature of the activator. Error bars indicate one standard deviation either side of the mean.

778
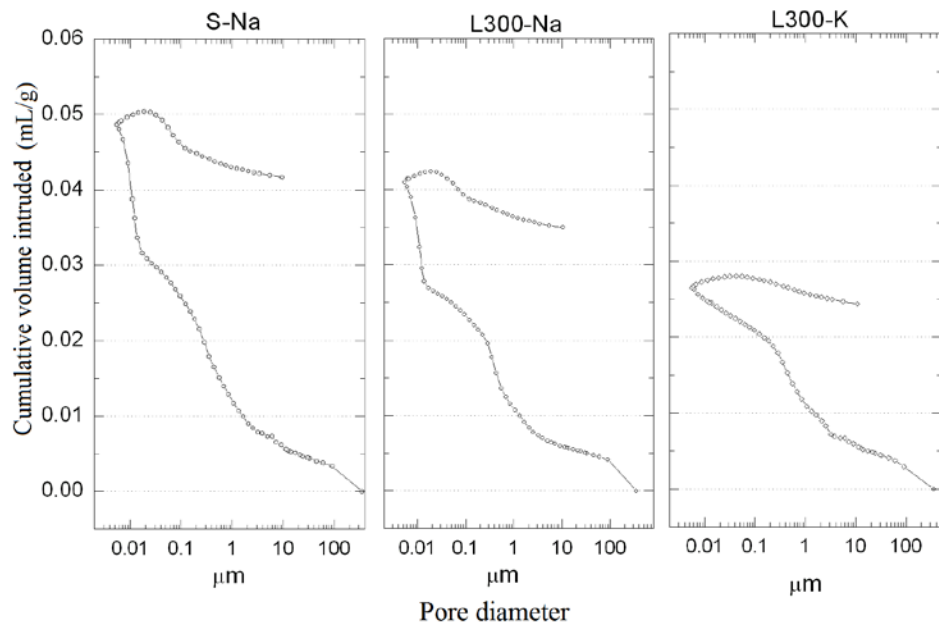
Figure 3. Cumulative volume of mercury intruded as a function of pore diameter for S-Na, L300-Na and L300-K mortars after 28 days of curing
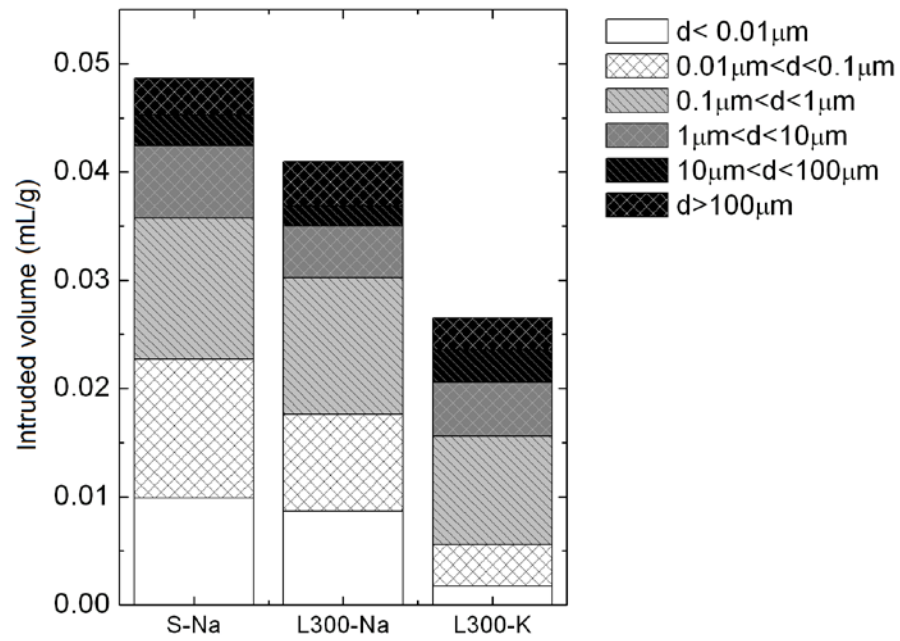
Figure 4. Pore size distributions obtained from mercury intrusion data for silicate-activated fly ash mortars with 28 days of curing

Figure 5. Cu-K$_\alpha$ diffractograms of the fly ash activated with Na-based activators. Peaks present in both diffractograms are labeled in only one diffractogram for visual clarity.

792

Figure 6. Cu-K$_\alpha$ diffractograms of the fly ash activated with K-based activators. Peaks
present in both diffractograms are labeled in only one diffractogram for visual clarity.

796

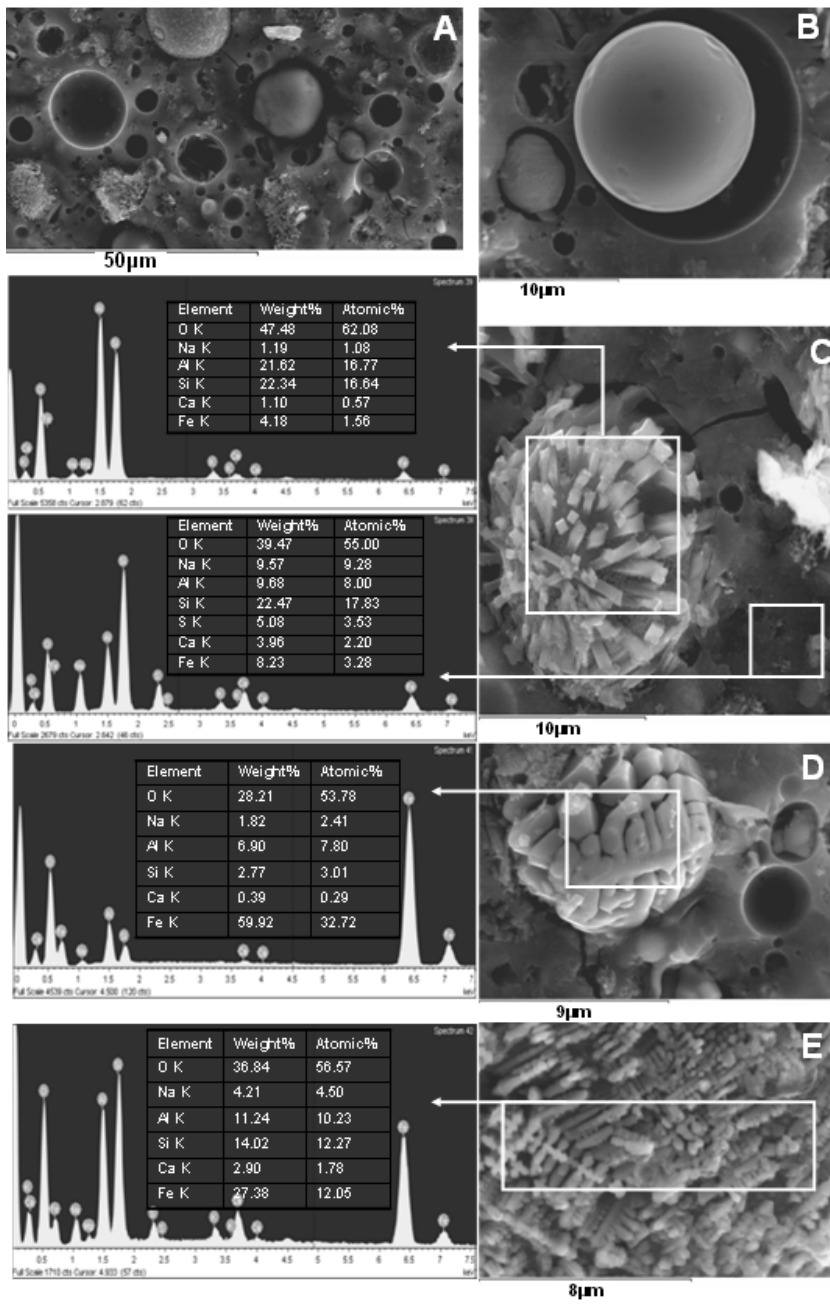797 **Figure 7.** Thermograms of silicate-activated fly-ash binders at 28 days of curing
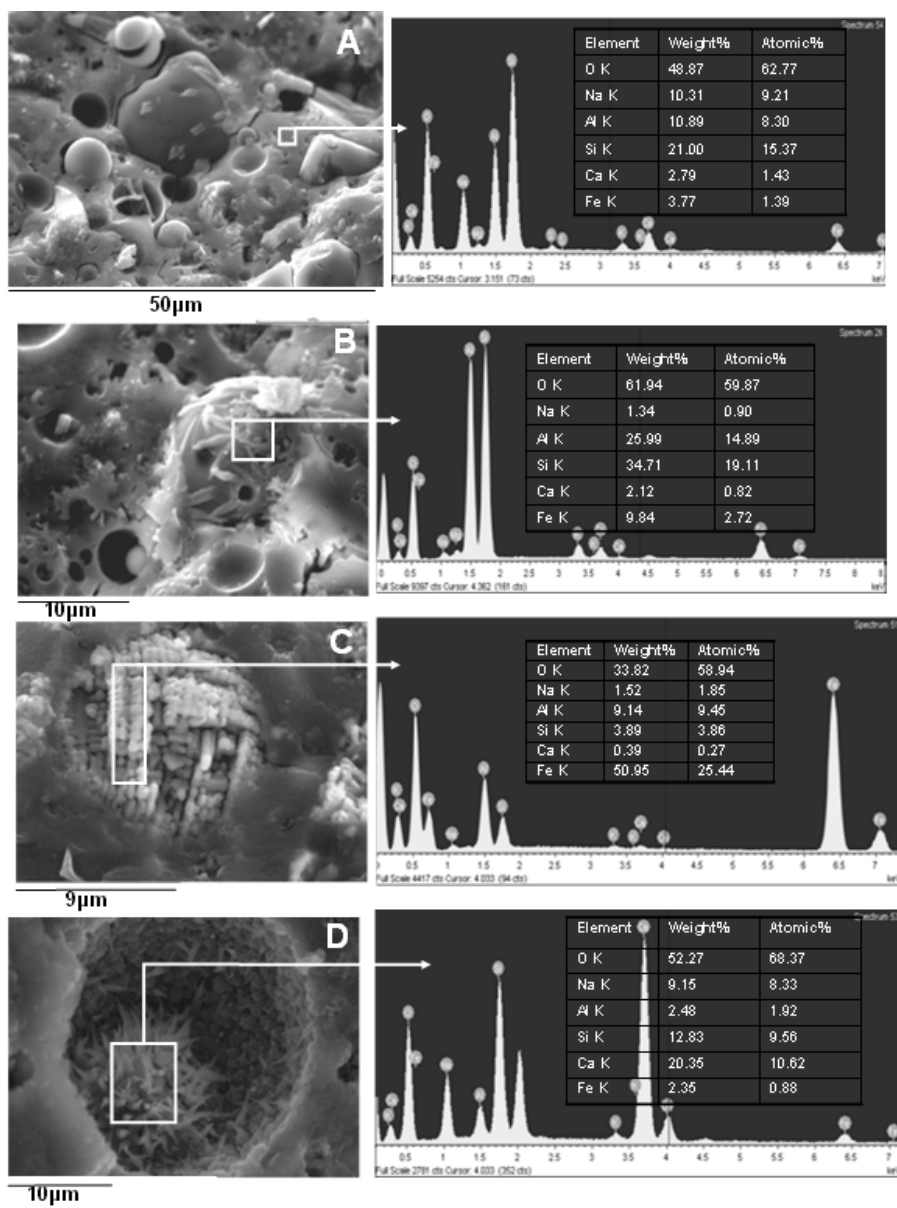
798
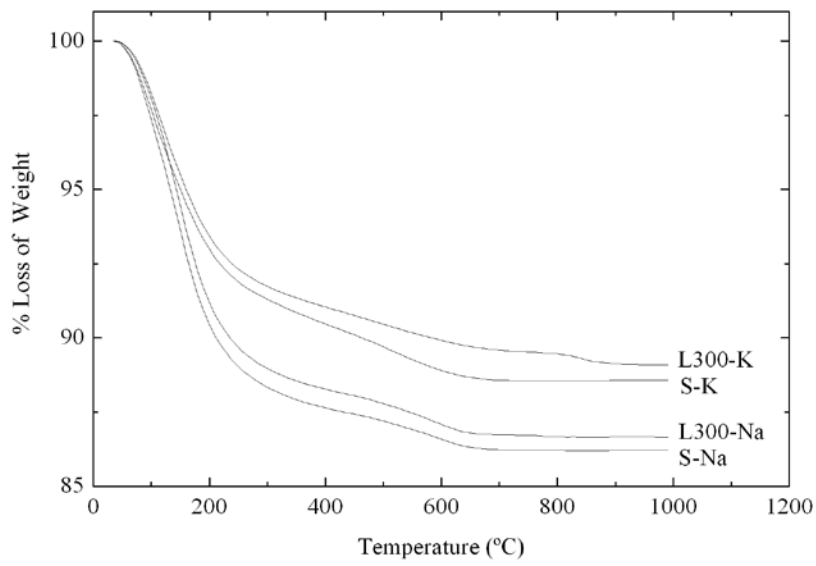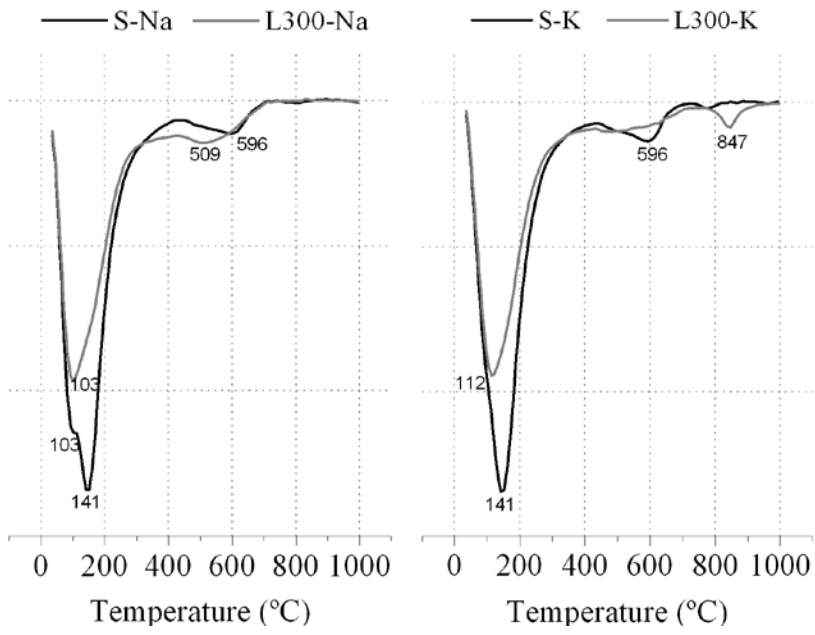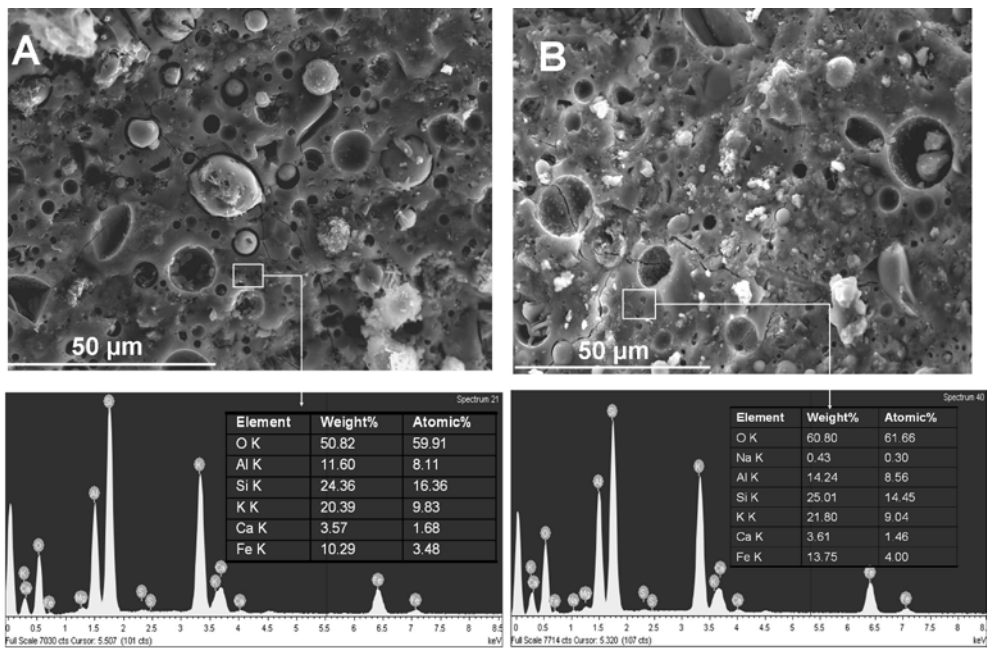
Figure 8. Differential thermograms of silicate-activated fly ash

Figure 9. Scanning electron micrographs and corresponding EDS spectra of the binder activated with a commercial sodium silicate (S-Na)

Figure 10. Scanning electron micrographs and corresponding EDS spectra for the binder
activated with NaOH/nanosilica-derived activator (L300-Na)

Figure 11. Scanning electron micrographs, and corresponding EDS spectra, of the binders activated with (A) commercial potassium silicate solution (S-K) and (B) KOH/nanosilica derived activator